

Conceptual Design of Floating Wind Turbines with Large-Amplitude Motion

Lei Wang

Department of Civil Engineering
Texas A&M University
Email: raywong@tamu.edu

Bert Sweetman

Department of Civil Engineering
Texas A&M University
Email: sweetman@tamu.edu

Abstract: The opportunity to reduce the hull size of spar-type floating offshore wind turbines is investigated in detail. Three conceptual designs based on the OC3-Hywind design are developed and analyzed, with drafts ranging from 84 m to the 120 m of the original OC3-Hywind. These substantial reductions in size correspond to meaningful increases in angular motion of the tower and rotor-nacelle assembly. Computed angular motions exceed the range for which conventional wind turbine analysis software is intended for use. A new time-domain simulation methodology is outlined. In the new method, accurate coupling between the various degrees of freedom is preserved. Rotational motions are computed using sequenced Euler angles and conservation of angular momentum and translational motions are computed using the theorem of motion of the mass center. Structural motions through the wind and water are included in the calculation of environmental forcing, such that the nonlinear coupling between forcing and response is preserved. Example analysis results are presented for both free and forced-vibration cases, and an estimate of structural efficiency is computed and expressed as power per unit weight structural steel, which is presented for each design alternative in a variety of wind conditions.

1 Introduction and Background

Environmental, aesthetic and political pressures continue to push for siting offshore wind turbines beyond sight of land, where waters tend to be deeper, and use of floating structures is likely to be considered. A major deepwater wind development would require large numbers of floating structures, which makes optimizing the structural configuration of these structures of primary importance. The first full-scale offshore floating wind turbine in the world, Hywind, has been installed in 2009 [1], which integrated a 2.3-MW turbine on a 65 m height tower. The base case of the investigation presented here is the OC3-Hywind, which is itself a conceptual design introduced by Jonkman [1] as an enlarged version of the installed 2.3-MW Hywind platform. The OC3-Hywind has a tower height of 87.6-m, supported by a 108-m underwater spar cylinder plus a taper and smaller cylinder for a total 120-m draft (Fig. 2). The design also includes a crowfoot structure to hold the mooring attachment points away from the cylinder axis to increase yaw stiffness. One design goal in this first floating structure was to minimize tower motion, which makes the technological leap from bottom-founded towers to floating structures relatively smaller. Much of the structural steel in the design is in the 108 m spar cylinder, the primary purpose of which is to maintain the tower in a near-vertical condition when subject to the very large horizontal wind force at the 77.6-m tall tower. Additional angular stability is provided through use of barite ballast in the bottom of the 120-m deep structure.

In this paper, alternate designs with reduced ballast weight and cylinder length are investigated. Reducing the ballast directly reduces the amount of buoyancy required to support the structure, and reducing the cylinder length directly reduces the required structural steel. Each of these modifications to the OC3-Hywind design are likely to reduce the cost of the structural steel; unfortunately, these design modifications also allow a much greater angle of tower lean for the same wind force. The increase in lean introduces some reduction in efficiency of energy harvesting, and the increased structural dynamics introduces an array of other technical concerns. Modeling of structural dynamics for these structures is particularly challenging, and important, because of the gyroscopic moments created by the huge whirling blades. For conventional, stiff, bottom-founded structures, these moments are primarily generated by mechanical precession of the spin axis into the shifting

winds, and so are limited by the maximum yaw rate [2]. However, no such limit exists for gyroscopic moments of floating structures because they result from irregular motions of the tower.

The computational challenges associated with these highly-compliant designs defy many existing simulation techniques: the wind forcing is irregular and non-linear; the wave forcing is irregular and nonlinear; the gyroscopic moments directly couple rotational degrees of freedom that can reasonably be assumed independent for other structural types, and large-angle motions defy the implicit assumptions underlying most computer-analysis methods. The well-recognized wind turbine dynamic analysis software, the NREL FAST aero-elastic simulator [3] [4], has been enhanced to include computation of hydrodynamic forces using WAMIT [5], which is also based on small-angle theory. Ideally, dynamic simulations should be based on properly sequenced Euler angles, but use of the Euler dynamic equations are difficult to implement using matrix methods commonly applied to multi-body systems.

Numerous solution techniques for multi-body dynamics problems are available. To mention a few, Stoneking (2007) [6] presents the derivation of the exact nonlinear dynamic equations of motion for a multi-body spacecraft connected by spherical gimbal joints. Saha (1999) [7] derives the constrained dynamic equations of motion using the decoupled natural orthogonal complement matrices for a serial kinematic chain composed of rigid bodies. H. Matsukuma et al. (2008) [8] employ multi-body dynamic system theory to analyze the dynamic response of a 2-MW downwind turbine mounted on a spar-type floating platform for pitch amplitudes up to around 10 degrees in steady wind, but no waves, and conclude that the platform motions are considerably influenced by gyro moments associated with rotor rotation.

The dynamic analysis on the alternate designs presented here applies a newly developing methodology that generalizes the conventional Euler dynamic equations of one rigid body to the equations of motion (EOMs) of the entire multi-body wind turbine system, including tower, rotor, nacelle and other moving parts. This method enables solution of the equations of motion using fewer degrees of freedom (DOFs) than would be required in a conventional finite element analysis (FEA) method. This enhanced numerical efficiency comes at the expense of neglecting the structural flexibility within each rigid body.

The technical challenges posed by these more compliant structural designs are significant, but meaningful weight savings could be realized, as can be demonstrated using simple dimensional analysis. Figure 1 shows the predominant loads on a spar-type floating wind turbine. Considering the static equilibrium of a tower subject to four constant forces representing each of these loads combined with the use of simple dimensional analysis yields considerable insight into the potential for weight savings. Other important forces such as waves and the water-plane stiffness are neglected from this very basic thought experiment. Considering just the four forces and arbitrarily defining pitch as the direction of the rotational motion caused by wind forces, pitch motion will be in static equilibrium if the couple created by the wind and mooring forces is equal to that of the buoyancy and gravity forces. The wind force and tower height are assumed to be approximately constant, which implies some constant wind moment must be reacted by buoyancy and gravity. A small increase in the design static pitch angle would allow either: 1) a decrease in the required buoyancy (B) and ballast weight, or 2) a decrease in the required restoring moment arm, which implies a decrease in the structural distance (D) between the center of gravity and center of buoyancy, or some combination of the two. Either option 1) or 2) implies a less weight structure. For sinusoidal motion, the amplitude of the inertial loads is the product of the moment of inertia, amplitude of the motion and the square of the circular frequency. Decreasing the stiffness reduces the pitch and roll natural frequencies, which decreases inertial loading. Simple dimensional analysis can also be used to investigate cost implications. Statically, the structure will pitch until the available restoring moment equals that created by the wind force. If the length is held constant, the available restoring moment is the buoyancy times the sine of the design pitch angle, $M \sim B \sin \theta \approx B\theta$, so for constant M , required buoyancy, $B \sim 1/\theta$. Alternatively, if the buoyancy is held constant and the length is allowed to vary, the available restoring moment varies linearly with the structural distance between the centers of buoyancy and gravity, $M \sim D\theta$, so required distance between the centers, $D \sim 1/\theta$. An extremely rough idea of the effect on cost could be inferred from approximate changes in steel weight associated with each of these changes because the cost highly depends on the weight of hull.

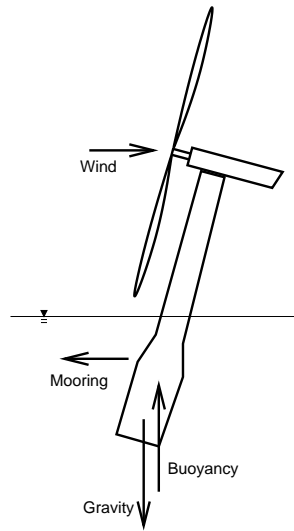


Fig. 1. Predominant forces on a floating wind turbine

This simple dimensional analysis provides some intuitive sense that an increase in the design pitch angle may result in lower weight structures, but the results of this over-simplified analysis need to be investigated by a more rigorous investigation. In this paper, three alternate conceptual designs are developed from the Original OC3-Hywind using unit weights and basic naval architectural principals. Each of four designs, the original OC3-Hywind plus the three new design alternates, are then analyzed to compare their dynamic performance and comparative energy harvesting efficiency.

2 Reduced Hull Designs

Three smaller conceptual designs are developed from the OC3-Hywind [1] by truncating the length of the spar cylinder and decreasing the ballast weight; the diameter of the cylinder remains constant for all four designs. The diameter of the upper small cylinder is 6.5-m; the diameter of lower large cylinder is 9.4-m. They are connected by a tapered structural cone, the height of which is 8-m. The main criterion for design is hydrostatic equilibrium: the available buoyancy provided by the spar hull must equal the weight of complete structure plus the vertical component of the top tension of the mooring lines. Buoyant volume and center of buoyancy calculations included the large cylinder, small cylinder and taper. Calculation of the physical weight includes the weights of hull and ballast plus the load associated with the mast supporting the rotor-nacelle assembly (RNA). For all designs, the diameter and the weight per length of the spar cylinder were held constant, and were based on the original OC3-Hywind design. Various combinations of length and ballast were investigated using a trial-and-error methodology to find three design alternatives that spanned a wide range of cylinder lengths and design pitch angles. The four conceptual designs selected for further analysis are outlined in Figure 2 and Table 1.

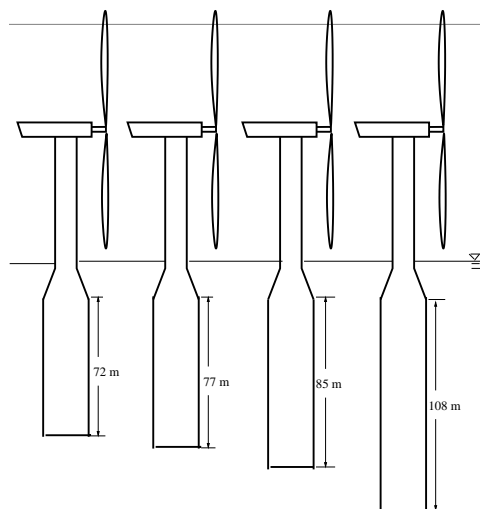


Fig. 2. Truncated Cylinder Designs

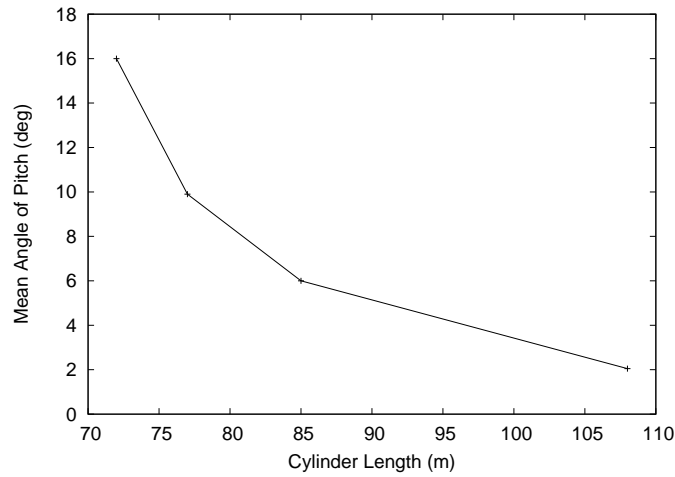


Fig. 3. Average pitch angle while operating in a 17 m/s Wind

The mean angle of pitch for each of these designs operating in a 17 m/s irregular wind combined with irregular seas is shown in Figure 3. The details of the dynamic analysis leading to this figure are presented later. The dynamic analysis of the floating structure subject to realistic irregular wind and waves shows that the floating structure finds a quasi-static equilibrium angles with relatively small dynamic motions about that position. The mean angles show range between about 2 and 16 degrees; the larger of those angles is well beyond any range for which small-angle assumptions are reasonable.

2.1 Investigation of the Small-Angle Assumption

The OC3-Hywind structure is analyzed in free vibration using two different analysis methods and two different sets of initial conditions. The first set of initial conditions is prescribed as 0.1 rad (≈ 5.7 degrees) in both roll and pitch, plus a horizontal offset in sway of 0.5 m at the mean sea level. Any yaw motion of the tower results from the gyro moments along the centerline of the tower. In conventional ship dynamic analysis, superposition of the six degrees of freedom (surge, sway, heave, roll, pitch and yaw) is assumed to be valid. However, for large angular motions, the order in which the rotational motions are applied matters. For example, a specific orientation in space results if a ship is moved through a large angle of roll, then a large angle of pitch applied at that roll angle, and finally a large angle of yaw is applied to the result; if the same roll, pitch and yaw angles are applied in a different order, a different final orientation in space will result. The physical implication of the mathematics underlying direct superposition of these angles implies that the axes of the (x, y, z) coordinate system are not mutually perpendicular; for small angles this implicit error is extremely small. Two different analysis methods are applied here. The first method is direct application of the well-known FAST computer program, which implies direct superposition of angular motions; the second method is a newly developing large-angle analysis tool called Loose which is based on large-angle theory in which angles are combined using sequenced Euler angles. In this analysis, mooring force is represented by two linear springs with stiffness equal to 5×10^4 N/m in the surge and sway directions such that precisely the same mooring system could be modeled in both FAST and Loose. The FAST user subroutine (UserPtfmLd) is used to apply the platform loading with calculation of hydrodynamics and mooring forcing being turned off. Additionally, tower flexibility in FAST has been disabled so the tower and rotor blades are modeled as rigid bodies in both methodologies, and hydrodynamic forcing has been disabled for the same reason. In the comparison, roll and pitch are assumed to be consistent with Euler angles X_4 and X_5 , which is reasonable for small angles [9]. Figures 4 and 5 demonstrate this equivalence, and also show that the new Euler-based method yields equivalent results as the well-proven FAST software. FAST is capable of modeling the system in considerably more detail than Loose: most notably, FAST considers the rotor and nacelle as two free

Table 1. Properties of Alternate Designs and Original OC3-Hywind

	Truncated			Hywind
Cylinder Length (m)	72	77	85	108
Platform Draft (m)	84	89	97	120
Hull Weight (tonnes)	816	860	940	unknown
Ballast (tonnes)	4,208	4,503	5,038	unknown
Total Platform Weight (tonnes)	5,024	5,363	5,978	7,466

bodies while loose considers them as a single rigid body, and Loose neglects all structural flexibility within the rigid bodies.

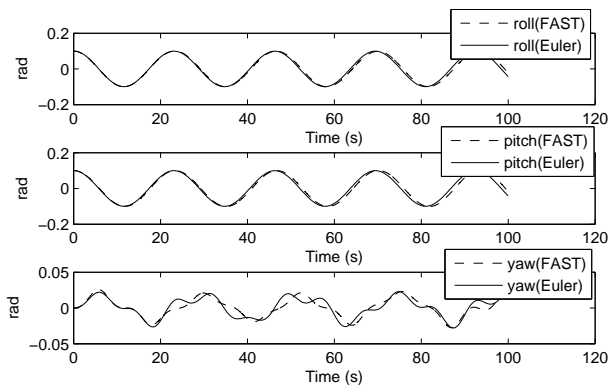


Fig. 4. Rotation comparison in case of small amplitude motion

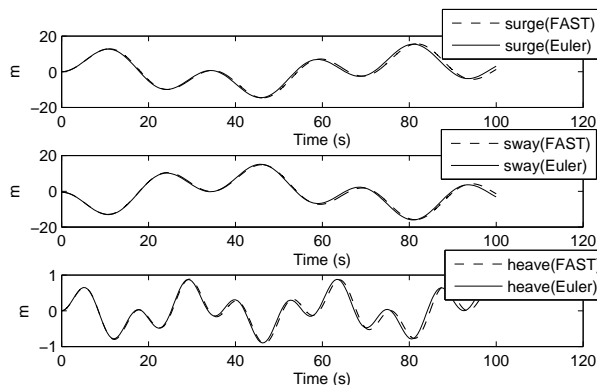


Fig. 5. Translation comparison in case of small amplitude motion

Figures 6 and 7 are similar to 4 and 5, but the initial conditions are considerably more severe: the initial pitch is 0.4 rad (23 degrees), and a constant horizontal force of 5×10^5 N is applied at the blade hub in the negative surge direction to simulate the wind force on an operating rotor. FAST has a built-in execution limit that causes execution to stop if hull pitch is excessive. That limit was disabled to allow this angle applied in this case to exceed the published angular limitations of FAST [4]. Additionally, this case is slightly non-physical in that the magnitude of the wind force is numerically preserved, but the spin rate of the blades is set to zero in both FAST and Loose to remove any gyroscopic effects. In this large-angle case, the details of the mathematical assumptions underlying FAST become relevant. The superposition of the rotational motions implies a non-normal coordinate system, which would generally result in non-orthonormal transformation matrices. Within FAST, a mathematical technique called the Frobenius Norm is applied to guarantee the orthogonality of transformation matrix. This technique effectively introduces very small non-physical changes to the coordinate system to guarantee mathematical consistency. These tiny errors are on the order of θ^3 , with θ in radians, and are inconsequential for the small angles for which FAST is intended; for large angles, however, these errors can accumulate over time and cause numerical instabilities. Figures 6 and 7 demonstrate this numerical instability when FAST is applied to conditions far beyond its intended limits. In particular, FAST shows an obvious increase in roll and yaw beginning about 50 seconds into the simulation. There is no forcing in the yaw or roll directions so these degrees of freedom should remain uniformly zero: the observed increase in the FAST simulation is entirely numerical and directly results from applying the software to a case far beyond its intended limitations. Results of the Euler-based methodology correspond to physical intuition.

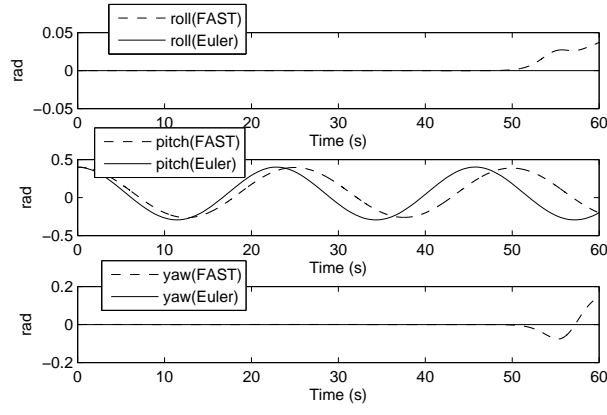


Fig. 6. Rotation comparison in case of large amplitude motion

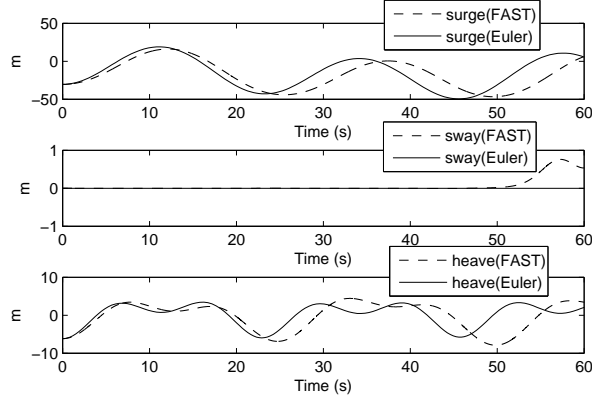


Fig. 7. Translation comparison in case of large amplitude motion

3 Loose: Coordinate Systems and Euler angles

The Euler-based methodology used to generate the various results presented here requires solving equations of motion in Euler-space. Several coordinate systems are used in the derivation of the global equations of motion, and transformations are developed such that external forcing can be projected onto the body coordinate systems, and body motions can be included in computation of these forces. The methodology considers the system as two rigid bodies: the tower is the complete structural assembly, including the buoyant hull, that supports the rotor-nacelle assembly (RNA); the RNA is the complete assembly that can mechanically yaw relative to the tower. It is reasonable to neglect structural flexibility for highly-compliant floating structures, because the global motions of these two bodies in space are much larger than the higher modes allowed by structural flexibility.

Fig. 8 shows that both the (X, Y, Z) and the (X_M, Y_M, Z_M) systems are earth-fixed global coordinate systems: (X, Y, Z) originates at the center of mass of the whole system and (X_M, Y_M, Z_M) originates at the mean still water plane of the undisturbed hull. The (x_t, y_t, z_t) and the (A, B, C) systems are body-fixed coordinate systems and originate at the CM of the tower and RNA, respectively. The CM of the RNA, G_R , is assumed to be on the centerline of the tower. The (x_s, y_s, z_s) system is parallel to (x_t, y_t, z_t) and originates at the instantaneous CM of the entire system, which is assumed to be on the centerline of the tower. Thus (x_s, y_s, z_s) coincides with (X, Y, Z) in absence of zero displacement.

The (X, Y, Z) and (x_s, y_s, z_s) coordinate systems are used for the application of theorem of motion of center of mass and theorem of moment of momentum on the entire system, respectively. Two body-fixed Cartesian frames, (A, B, C) and (x_t, y_t, z_t) , are assumed to be composed of principal axes of inertia in order to simplify the calculation of angular momentum of the two rigid bodies. The (X_M, Y_M, Z_M) system is defined to compare simulation results with those of FAST, which has standard reference point prescribed to be on the mean sea level.

Fig. 9 introduces the Euler angles to describe large-amplitude rotational motion. For large angular displacements in space, the order in which the angles of rotation are applied is important; there are twelve possible Euler angles sequences. Six of the 12 combinations have two repeated rotational axes (e.g. 3-1-3), while the other six have three different rotational axes (e.g. 1-2-3). The 1-2-3 sequenced Euler angles are the most commonly used in part because they are nearly equivalent

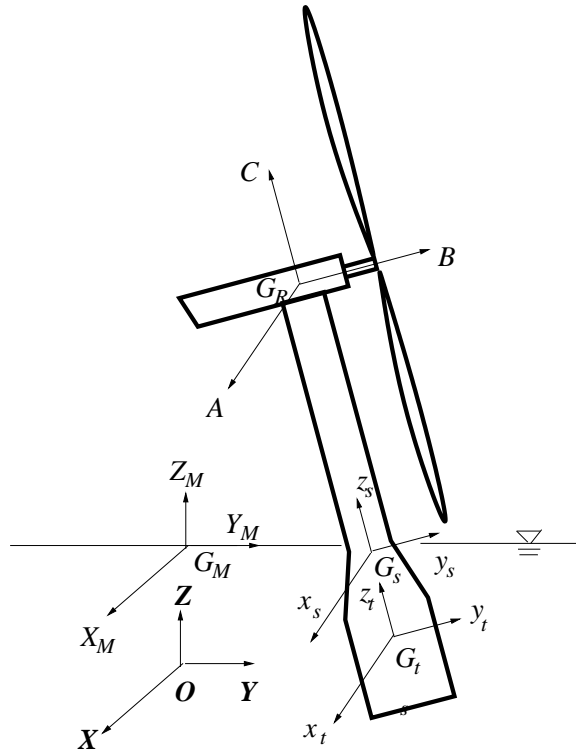


Fig. 8. Coordinate systems used in the application

pitch-roll-yaw for small-amplitude motion [9]. Here, the 1-2-3 sequenced Euler angles X_4 - X_5 - X_6 are used to describe the position of the rotating tower. The (x', y', z') is translating coordinate system with respect to the (X, Y, Z) system, with the origin located at the CM of the tower. The (x_t, y_t, z_t) system can be transformed from the (x', y', z') by: first rotating the upright tower about the x' -axis by angle X_4 ; and then rotating about the resulting second coordinate axis through an angle X_5 ; finally, rotating the tower about the z_t -axis through the third Euler angle, X_6 .

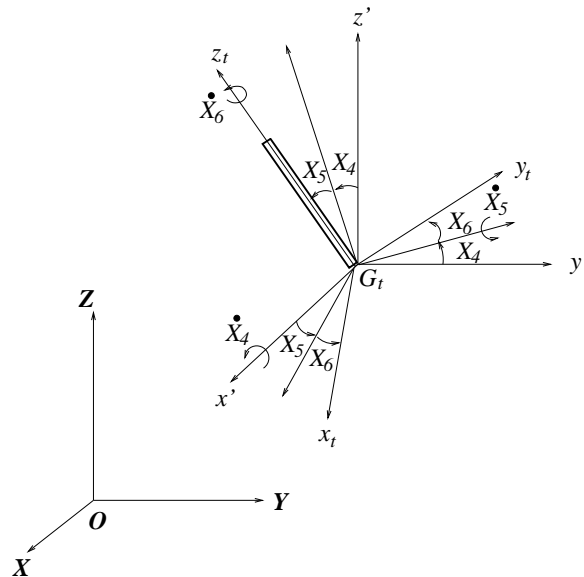


Fig. 9. 1-2-3 sequenced Euler angles in terms of X_4 , X_5 and X_6

4 Loose: Equation of Motion of the System

Conventional derivation of the Euler equations of motion are based on conservation of angular momentum applied to one rigid body; here, the theorem of moment of momentum is directly applied to a system of two bodies: the RNA and

tower. The nacelle yaw rate is the angular motion between them. The exact moments of inertia of the RNA are preserved in the (A, B, C) coordinate system. The entire RNA is assumed to be spinning.

Beginning at first principles, the sum of the moments resulting from externally applied forces about the center of mass of a system of particles in the translating-rotating system, (x_s, y_s, z_s) , equals the change of amplitude of the momentum within the coordinate system plus the change of direction of the momentum with respect to global coordinate system (e.g. [10]):

$$\sum \vec{M} = \dot{\vec{H}}_{G_s}^s = (\dot{\vec{H}}_{G_s}^s)_{x_s, y_s, z_s} + \vec{\omega}_t \times \vec{H}_{G_s}^s \quad (1)$$

The L.H.S. of Eqn. (1), $\sum \vec{M}$, represents the moments from all of external forces, including environmental forcing and restoring forcing; $\vec{H}_{G_s}^s$ is the angular momentum of the entire multibody system calculated about the CM of that system. Vector $\vec{H}_{G_s}^s$ is decomposed into the (x_s, y_s, z_s) system, which has the same angular motion as the tower, $\vec{\omega}_t$, because the G_s and G_t coordinate systems both rotate with the same rigid tower. It is therefore convenient to use $\vec{\omega}_t$ to describe the angular velocity of the system (x_s, y_s, z_s) with respect to global coordinate system (X, Y, Z) . Total momentum $\vec{H}_{G_s}^s$ results from superimposing the momenta of all rigid bodies within the system:

$$\vec{H}_{G_s}^s = \vec{H}_{G_s}^R + \vec{H}_{G_s}^t \quad (2)$$

where the angular momentums of RNA and tower in the (x_s, y_s, z_s) system, $\vec{H}_{G_s}^R$ and $\vec{H}_{G_s}^t$, are calculated about the CM of the system, G_s , which can be further related to the angular momentums about the CM of these two rigid bodies, $\vec{H}_{G_R}^R$ and $\vec{H}_{G_t}^t$, by means of the theory of angular momentum about an arbitrary point [9]. Assigning the body-fixed coordinate system (x_t, y_t, z_t) to the principal axes of inertia of the tower, the angular momentum of the tower can be obtained by first calculating the product of the principle inertia tensors axes and the angular velocity of the tower and then transforming the result into the (x_s, y_s, z_s) system:

$$\vec{H}_{G_t}^t = T_{t \rightarrow s}(I_t \vec{\omega}_t) \quad (3)$$

where $T_{t \rightarrow s}$ is the transformation matrix from (x_t, y_t, z_t) to (x_s, y_s, z_s) and equal to the elementary matrix because these two coordinate systems are parallel; I_t is the inertia tensor of the tower and is in the form of diagonal matrix with elements equal to the moments of inertia of the tower about corresponding principal axes. In Eqn. (3), the absolute angular velocity of the tower, $\vec{\omega}_t$, is decomposed into the body fixed coordinate system (x_t, y_t, z_t) and can be represented in terms of 1-2-3 sequenced Euler angles by [11]:

$$\vec{\omega}_t = \begin{bmatrix} \dot{X}_4 \cos X_5 \cos X_6 + \dot{X}_5 \sin X_6 \\ -\dot{X}_4 \cos X_5 \sin X_6 + \dot{X}_5 \cos X_6 \\ \dot{X}_4 \sin X_5 + \dot{X}_6 \end{bmatrix} \quad (4)$$

Similarly, the (A, B, C) axes are also assumed to be the principal axes of the RNA. To calculate the angular momentum of the RNA, $\vec{H}_{G_R}^R$, the angular velocity of the nacelle within the (A, B, C) system, $\vec{\omega}_n$, should be obtained by first calculating it in the (x_t, y_t, z_t) system in terms of nacelle yaw rate w.r.t. tower and then transforming into the (A, B, C) system. Thus, the angular momentum of the RNA can be expressed:

$$\vec{H}_{G_R}^R = T_{R \rightarrow s}(I_R \vec{\omega}_n) + T_{R \rightarrow s} I_R \dot{\vec{\psi}} \quad (5)$$

where I_R is the inertia tensor of RNA in the form of diagonal matrix; the spinning vector $\dot{\vec{\psi}}$ has a positive component along the B -direction, i.e. $\dot{\vec{\psi}} = (0, \dot{\psi}, 0)$; the transformation matrix from (A, B, C) to (x_s, y_s, z_s) , $T_{R \rightarrow s}$, is a function of the yaw angle of the nacelle, which is the rotation of (A, B, C) relative to some arbitrary initial angle between the B - and y_s -axes.

Eqn. (1) can be further expanded to investigate the gyro moments, which result from the time derivative of angular momentum associated with the spinning rate, and can be shown in the (A, B, C) system as $M_{G_R}^{gyro} = (-I_B \dot{\psi} \omega_{n,C}, 0, I_B \dot{\psi} \omega_{n,A})$ with $\omega_{n,B}$ and $\omega_{n,C}$ equal to two components of angular velocity of the RNA in the (A, B, C) system. The cross product in the equations of motion results in the transfer of angular momentums: the angular velocity component of the nacelle in the C -direction is related to the component of gyro moments in the A -direction, M_{gyroA} ; the angular velocity component of the nacelle in the A -direction is related to the component of gyro moments in the C -direction, M_{gyroC} . These results are in

agreement with the conventional gyroscopic moment calculation for a vertical tower. In that case, the angular velocity of the nacelle is always along the C -axis and equal to the yaw rate, ω_{yaw} . For a vertical tower, the gyro moments can reduce to the familiar $(I_B \dot{\psi} \omega_{yaw}, 0, 0)$ [12].

Locating the center of coordinate system at the center of mass of the entire system enables traditional Newtonian equations of motion to be applied to the translation of the systems. The theorem of the motion of the center of mass is applied to the entire wind turbine system to solve the translational DOFs: $\sum \vec{F} = m_s \vec{a}_{G_s}$, where \vec{a}_{G_s} is the linear acceleration of the CM of the system, $\vec{a}_{G_s} = (\ddot{X}_1, \ddot{X}_2, \ddot{X}_3)$; m_s is the mass of the whole system; the force vector $\sum \vec{F}$ represents the external forces of the entire system in the inertia coordinate system (X, Y, Z) , including environmental forces, restoring forces and gravity.

5 Loose: Restoring Forcing

The restoring forces and moments of the system result from the contribution of hydrostatics and mooring lines. All of these forces and moments must be calculated about the C.G. of the system, G_s , in order to be consistent with application of the theorem of the moment of momentum to that system. The center of the system may experience large excursions from the original equilibrium position, especially in case of large-amplitude motion of the tower. Accurate motion simulations require that these large excursions be considered in both hydrostatic and mooring line force calculations.

Hydrostatic restoring forces result from static buoyancy. The buoyancy of the circular cylindrical floater in the inertial coordinate system (X, Y, Z) is first calculated by $\vec{F}_B^I = (0, 0, \rho g \pi r^2 h_1)$, where ρ is the density of sea water; g is the gravitational acceleration; r is the radius of the cylinder; h_1 is instantaneous submerged length of the cylinder along the centerline. The center of buoyancy of a submerged circular cylinder (only) can be expressed by [11]:

$$\begin{aligned} x_s^B &= -\frac{t_{31} r^2}{4t_{33} h_1} \\ y_s^B &= -\frac{t_{32} r^2}{4t_{33} h_1} \\ z_s^B &= \vec{h}_G + \frac{h_1}{2} + \frac{r^2(t_{31}^2 + t_{32}^2)}{8t_{33}^2 h_1} \end{aligned} \quad (6)$$

where vector \vec{h}_G indicates the position of the bottom of the cylinder measured from the (x_s, y_s, z_s) system along the centerline; t_{31} , t_{32} and t_{33} are three elements in the transformation matrix from (x_s, y_s, z_s) to (X, Y, Z) : $T_{s \rightarrow I} = T_x(X_4)T_y(X_5)T_z(X_6)$, where $T_x(X_4)$, $T_y(X_5)$ and $T_z(X_6)$ are element transformation matrix [13]. By defining radius vector $\vec{\rho}_{B/G_s} = (x_s^B, y_s^B, z_s^B)$, the hydrostatic restoring moment is $\vec{M}_{hydro}^s = \vec{\rho}_{B/G_s} \times \vec{F}_B^s$, where the buoyancy in the (x_s, y_s, z_s) system can be obtained by using transformation matrix from (X, Y, Z) to (x_s, y_s, z_s) : $\vec{F}_B^s = T_{I \rightarrow s} \vec{F}_B^I$.

The mooring system is represented as neutrally buoyant taut tethers such that tension changes due to fairlead offsets result from only the elasticity of the line. Assuming the radius position of the fairlead of one mooring line in the (x_s, y_s, z_s) system is $\vec{\rho}_{A/G_s}$, the position of this fairlead (point A) in the inertia coordinate system (X, Y, Z) is: $\vec{\rho}_{A/O} = \vec{\rho}_{G_s/O} + T_{s \rightarrow I} \vec{\rho}_{A/G_s}$, where the radius vector $\vec{\rho}_{G_s/O}$ is the position of G_s measured from the (X, Y, Z) system, $\vec{\rho}_{G_s/O} = (X_1, X_2, X_3)$. The position of the fixed end (point E) of this mooring line on the sea bottom, $\vec{\rho}_{E/O}$, can be measured easily from the (X, Y, Z) system because it is constant and not function of time. Thus, the radius position from point A to point E in the (X, Y, Z) system is $\vec{\rho}_{E/A} = \vec{\rho}_{E/O} - \vec{\rho}_{A/O}$. The tension along this taut line in the (X, Y, Z) system can be obtained by the nature of elasticity material [11]:

$$\vec{F}_{line}^I = [T_0 + \frac{ES}{L}(\rho_{E/A} - L)] \frac{\vec{\rho}_{E/A}}{\rho_{E/A}} \quad (7)$$

where T_0 is the pretension of this mooring line; E is Young's Modulus; S is the cross sectional area of the line; L is the initial length of the line; $\rho_{E/A}$ is the norm of the vector $\vec{\rho}_{E/A}$, i.e. the instantaneous length of the line. This formulation would not apply to conventional catenary mooring lines. Similar to the hydrostatic restoring moment, the mooring line moment in the (x_s, y_s, z_s) system can be obtained by using a transformation matrix. The contribution of each mooring line can be calculated consecutively and then summed.

6 Loose: Environmental Forcing

A simplified method of computing the environmental loading on the blade area is used in place of more advanced and rigorous calculation of the aerodynamic loading which would normally include effects such as dynamic wake and

stall. Here, a simple approximation of the wind force in the (X, Y, Z) system and wind moment calculated about G_s in the (x_s, y_s, z_s) system are computed for use in the equations of motion. The rotor thrust force resulting from wind is approximately (e.g., [14]):

$$F_b = \frac{1}{2} C_T \rho_a A_b V_{rb}^2 \quad (8)$$

where ρ_a is the density of air; A_b is the swept area of the blades; C_T is the thrust coefficient; V_{rb} is the amplitude of the velocity of the wind relative to the RNA along the B -axis including tower motions. The wind force is assumed to be applied on the center of the blades area and along the B -axis, with lateral wind loads neglected, i.e. wind force is perpendicular to the blade area. This thrust force is computed as a function of thrust coefficient, C_T , which depends solely on relative wind velocity and is taken directly from Nielsen [14] and copied in Fig. 10. This curve is a simplified representation of the influence of conventional blade pitch control on the thrust, which maximizes the power output before cut-in speed (8.7 m/s here) and retains constant power output after cut-in speed.

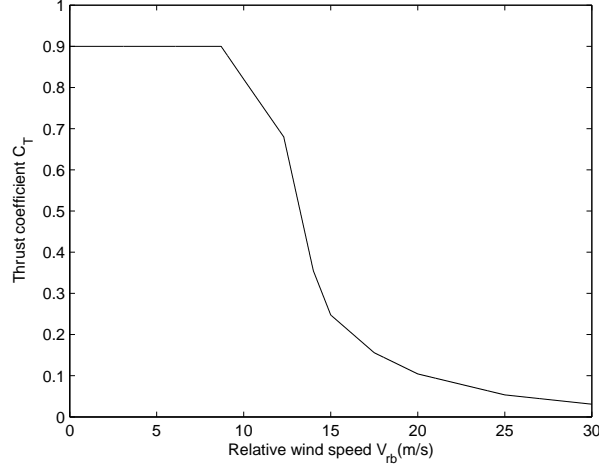


Fig. 10. Thrust force coefficient as function of relative wind velocity([14])

The amplitude of relative velocity, V_{rb} , can be computed by projecting both the wind velocity and structural velocity on the B -axis. Thus, a unit vector in the (X, Y, Z) system, \vec{u}_B^I , is used to indicate the direction of the B -axis by $\vec{u}_B^I = T_{R \rightarrow I} \vec{u}_B^R$, where \vec{u}_B^R is the unit vector along B -axis in the (A, B, C) system, i.e. $\vec{u}_B^R = (0, 1, 0)$; the transformation matrix from (A, B, C) to (X, Y, Z) , $T_{R \rightarrow I}$, can be obtained by the multiplication of transformation matrices: $T_{R \rightarrow I} = T_{S \rightarrow I} T_{R \rightarrow S}$. In Fig. 8, ignoring the distance between G_R and the center of the hub, the structural velocity of the center of blades area can be expressed as: $\vec{V}_{G_R}^I = \vec{V}_{G_s} + T_{S \rightarrow I} (\vec{\omega}_I \times \vec{\rho}_{G_R/G_s})$, in which \vec{V}_{G_s} is the linear velocity of G_s in the inertial coordinate system (X, Y, Z) ; the radius vector $\vec{\rho}_{G_R/G_s}$ is originated from G_s to G_R . Thus, the amplitude of relative wind velocity can be obtained by $V_{rb} = V_w - V_b = \vec{V}_{wind}^I \cdot \vec{u}_B^I - \vec{V}_{G_R}^I \cdot \vec{u}_B^I$, where \vec{V}_{wind}^I is the wind velocity in the (X, Y, Z) system. The wind force in the (X, Y, Z) system can be expressed as $\vec{F}_{wind} = T_{R \rightarrow I} \vec{F}_{wind}^R$, where \vec{F}_{wind}^R is the wind force in the (A, B, C) system, i.e. $\vec{F}_{wind}^R = (0, -F_b, 0)$. The wind moment in the (x_s, y_s, z_s) system is $\vec{M}_{wind} = \vec{\rho}_{G_R/G_s} \times \vec{F}_{wind}^R$.

Similar to the calculation of restoring forcing, wave forces are computed in the (X, Y, Z) coordinate system and then decomposed into the (x_s, y_s, z_s) system in order to compute the moments. The generalized Morison equation is applicable to cylindrical structures sufficiently slender relative to the wavelength that they can be assumed not to affect the incident waves; a common criteria is that the diameter of cylinder be less than 1/5 of the incident wavelength. For larger floating bodies, radiation-diffraction theory is generally applied. Using the Morison equation, the wave force per unit length of the inclined cylinder is (e.g., [15]):

$$\vec{f}_n^I = C_m \rho \frac{\pi}{4} D^2 \ddot{V}_n - C_a \rho \frac{\pi}{4} D^2 \dot{V}_t + \frac{1}{2} \rho C_d D \vec{V}_{rt} |\vec{V}_{rt}| \quad (9)$$

where ρ is the density of sea water; D is the diameter of the tower; C_m is the inertia coefficient; C_a is the added mass coefficient, and C_d is the drag coefficient. All velocities and accelerations are normal to the central axis of the tower: \dot{V}_n is the normal component of wave acceleration; \dot{V}_t is the normal component of structural acceleration; \vec{V}_{rt} is component of water particle velocity relative to the cylinder.

The normal direction of the wave kinematic vectors requires determination of unit vector $\vec{e}_3^t = (0, 0, 1)$ is along the central axis of the tower in the (x_t, y_t, z_t) system. Transforming to the (X, Y, Z) system, the normal component of water particle acceleration can be expressed as: $\vec{V}_n = \vec{e}_3^t \times (\vec{V} \times \vec{e}_3^t)$, where \vec{V} is the wave acceleration vector in the (X, Y, Z) system. Similarly, the wave kinematic velocity relative to the moving tower, \vec{V}_{rt} , can be expressed as: $\vec{V}_{rt} = \vec{e}_3^t \times (\vec{V}_r \times \vec{e}_3^t)$, where \vec{V}_r is the relative velocity of the wave to the segment of the submerged tower. The total wave force on the cylinder is obtained by summing up the force on each segment from Eqn. (9). Wave moments in the (x_s, y_s, z_s) coordinate system are computed by transforming the resulting forces from Eqn. (9) into the (x_s, y_s, z_s) system and then numerically integrating over the submerged length of the tower: $\vec{M}_{wave} = \int_r [\vec{\rho}_{i/G_s} \times (T_{I \rightarrow s} \vec{f}_n^I)] dr$.

7 Example: Loose simulations subject to irregular environmental loads

All of the examples presented in this section apply the Euler-based simulation methodology to the shortest of the spar-based floating wind turbines (84m draft), described in Table 1. Environmental loading is computed using irregular winds and waves along the negative direction of Y -axis. Irregular wind velocities are simulated by TurbSim [16]. Wave forces are computed using the Morison equation and a first-order time-domain representation of irregular waves is simulated directly from a JONSWAP spectrum with a significant wave height of 5.0 m and peak period of 12 s using a uniform phase distribution.

7.1 Dynamic behavior of a highly compliant spar

The dynamic behavior of the truncated spar is analyzed and shown to be meaningfully influenced by the blade-pitch control strategy. The present implementation of the Euler-based simulation method does not have any advanced control simulation capability and development of a pitch-control algorithm for highly compliant wind turbines has not yet been investigated. In the dynamic studies presented here, the possible control algorithms are bounded by two extremes. Optimal energy harvesting should result from ideal blade-pitch adjustments in which the blade pitch is adjusted instantaneously to the apparent wind velocity relative to the moving tower. Here, that strategy is implemented by applying Equation 8 with the thrust coefficient, C_t , updated at every time step based on the computed apparent wind and Figure 10. These very rapid blade-pitch adjustments may not be realistically practical in the field. At the other extreme from instantaneous adjustment is to set the coefficient of thrust based on Figure 10 using the mean wind speed and leave it at that fixed value throughout the simulation.

Fig. 11 shows both wind velocity and the relative wind velocity perpendicular to the blades area. Figs. 12 and 13 show tower motions in each of its 6 DOF with application of the instantaneously variable thrust coefficient. Comparison between these figures and Fig. 14 shows the effect of a fixed thrust coefficient corresponding to a fixed 17 m/sec wind velocity: positive damping is introduced; similar results are discussed in [14]. Fig. 15 shows a time-history of the gyro moments along A - and C -directions. M_{gyroA} and M_{gyroC} routinely have magnitudes of around 5×10^6 N-m and 1×10^6 N-m respectively, which cannot safely be ignored in design. Fig. 16 shows the pitch motion of floating wind turbine in hurricane conditions with mean wind velocity of 36m/s and a significant wave height of 14.4 m and the rotor parked. The wind load on the blades is dramatically reduced for the parked condition; wind force on the blades is computed using Eqn. (8) with $C_D=0.0025$ and the blades swept area replaced by frontal area of three blades. The maximum pitch angle found is around 6 deg , which is substantially less than in normal operations without consideration of controller-induced instability and wind loads on the tower.

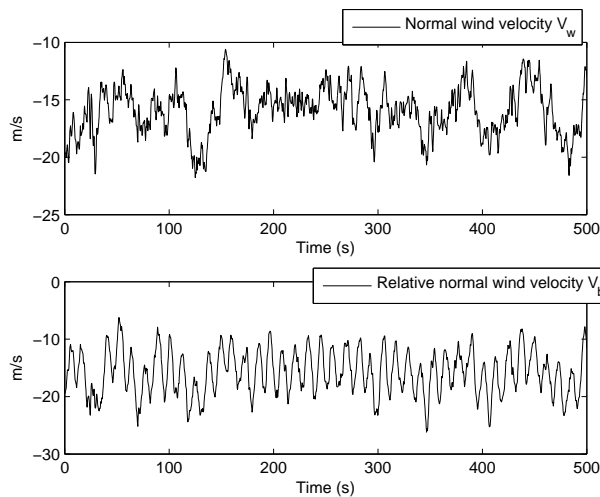


Fig. 11. Normal wind velocity and relative wind velocity

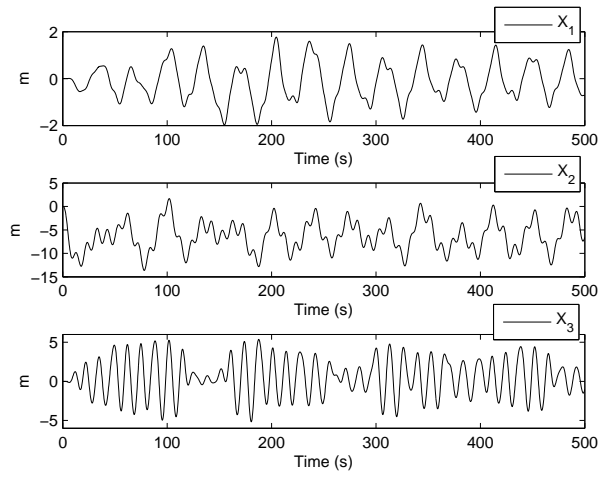


Fig. 12. Translational motion with variable coefficient of thrust

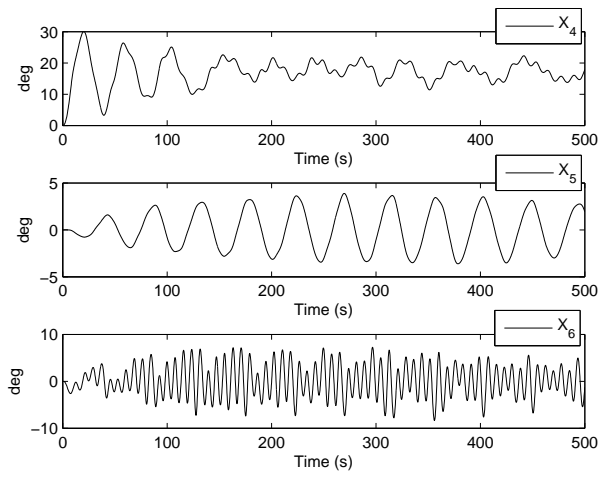


Fig. 13. Rotational motion with variable coefficient of thrust

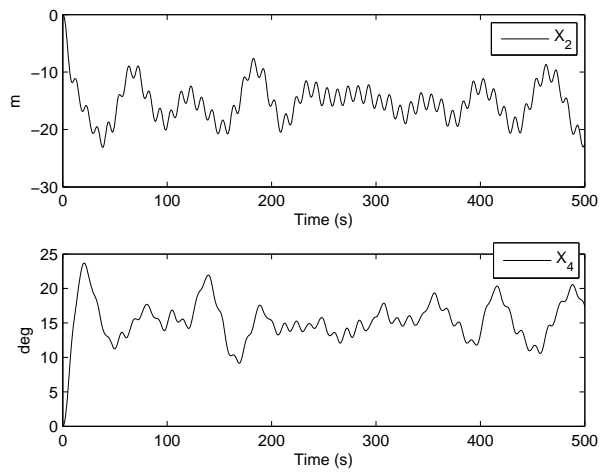


Fig. 14. Surge and pitch with fixed Coefficient of thrust

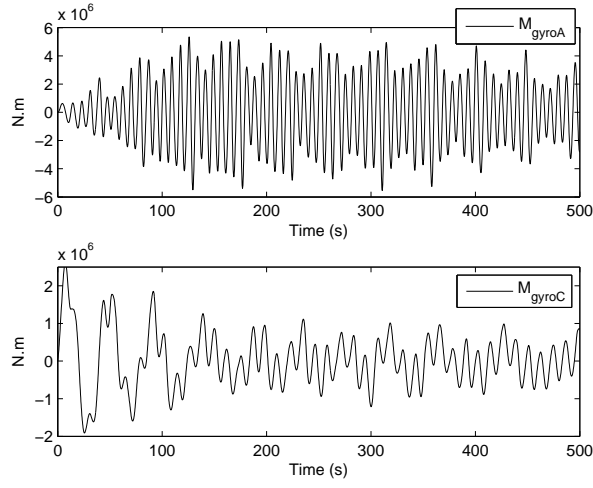


Fig. 15. Gyro moments with variable coefficient of thrust

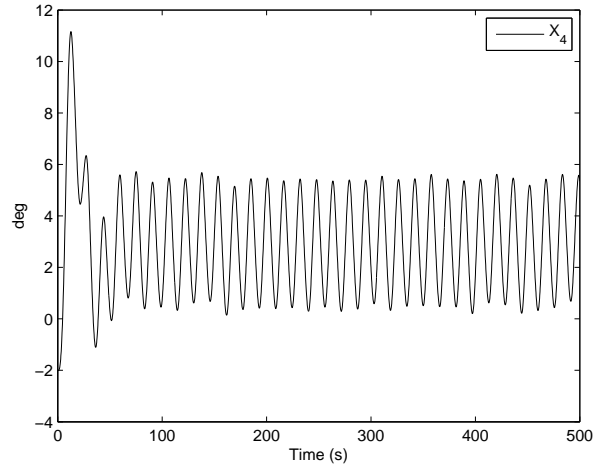


Fig. 16. Pitch motion in case of hurricane

7.2 Performance of various cylinder lengths

The four designs outlined in Table 1 and Fig. 2 are analyzed to assess their global behavior and relative efficiency. Figure 17 shows both the mean and standard deviation of the platform pitch for each of the four competing designs with the standard deviation magnified by a factor of 10. The figure was generated by combining results of 10 realizations of a 180-minute irregular sea state and irregular wind time histories, using the same wind and wave time histories for each of the bounding blade-pitch control strategies: fixed vs variable C_T . The four sets of combined wind-wave conditions used here are taken directly from Nielsen [14]: mean wind velocities of 8 m/s, 17 m/s, 20 m/s, 25 m/s with corresponding wave conditions of significant wave heights 3 m, 5 m, 9 m, 14 m and peak periods 10 s, 12 s, 13 s, 15 s, respectively. The wind and wave process are assumed to be stationary for the full 180-minutes. The reference height for the four specific wind speeds is 87.6 m (hub height).

Considering the results shown on Figure 17, mean platform pitch angle shows the expected increase with decreasing cylinder length. The general behavior of these compliant systems is to have a large, relatively steady mean offset and dynamic variation about that mean. The standard deviation shown is the square root of the variance of the process, and therefore indicates the magnitude of the dynamic motions about the mean. It also appears that increasing tower pitch corresponds to greater difference between the fixed- and variable C_T cases. This effect probably results from computing the inflow velocity in the variable C_T cases as the component of velocity perpendicular to the blade area, so for large angles, the average C_T in the variable C_T cases corresponds to a lower average inflow velocity than that of the fixed C_T cases. Greater differences between the two control strategies can also be seen at the 17 m/sec rated wind speed than at other speeds, presumably because the slope of C_T curve in Fig. 10 is steepest near the rated wind speed. The general trend for the fixed C_T cases is to have smaller standard deviation than fixed results from the greater aerodynamic damping, as also noted in [14].

For each of the time-history realizations of the rated wind case, the power output is calculated as $P = \frac{1}{2} C_p \rho_a A_b V_{rb}^3$ [14],

where A_b is the swept area of the blades; C_p is a power coefficient ($C_p = 0.7C_T$), which guarantees that output power of OC3-Hywind model is 5-MW. The results of the power calculation are presented as Fig. 18, which shows the ratio of the hull structural weight to the output of power. Results presented here explicitly consider platform motions in the power calculation. Designs with greater platform pitch angles generate slightly less power because the inflow velocity perpendicular to the blades is slightly reduced (or, equivalently, the projected area of the blades perpendicular to the wind is slightly reduced). Here the power is computed as 4.16 MW, 4.53 MW, 4.76 MW, 5.0 MW. The slight decrease in energy harvesting efficiency is counter-balanced by decreased structural weight. The most effective design is that with the lowest weight per KW. The figure also shows a substantial difference between the harvesting efficiency of the fixed versus variable C_T cases. This result emphasizes the importance of optimal control system design. The energy harvesting effectiveness of a wind turbine with a realistic blade pitch control system is expected to be between these two extremes.

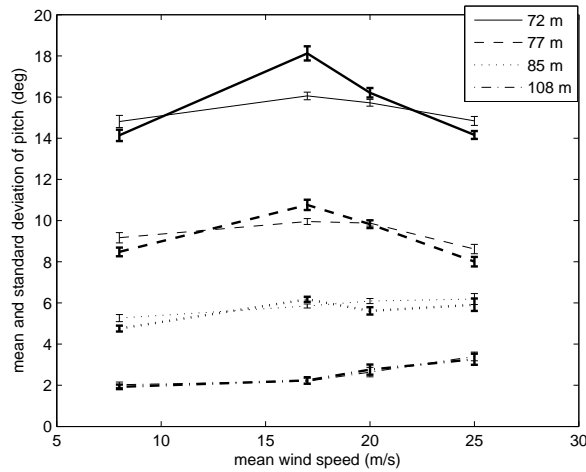


Fig. 17. Platform pitch for various cylinder lengths and blade-pitch control strategies (heavy lines indicates variable C_T)

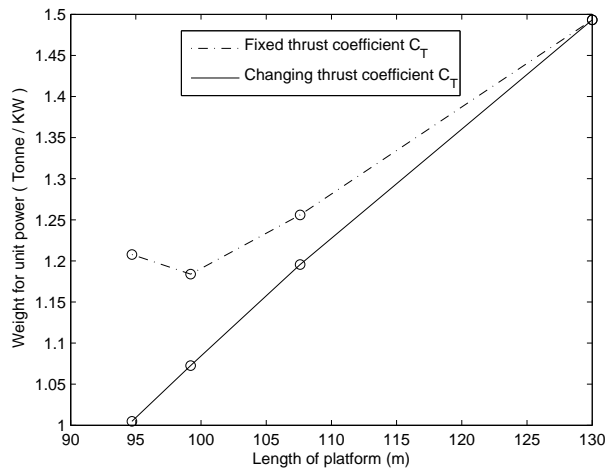


Fig. 18. Weight of supporting structure per unit power output

8 Conclusions

Four alternate spar-based floating wind turbine designs have been analyzed and compared in terms of rigid-body dynamics and energy harvesting efficiency. The first of these designs is the OC3-Hywind, and the remaining three are developed by shortening the spar hull and reducing the ballast of the Hywind design. The large-angle motions inherent to the shorter spar designs defy the mathematical assumptions underlying common wind turbine analysis tools, so a new methodology based on Euler angles is introduced. Worked examples are used to show the effectiveness of the analysis and the relative performance of the truncated spar designs. It is found that the smaller floaters have much larger mean offsets, but only slightly larger dynamic motions around these means. It is also found that there is a significant opportunity for improved efficiency through use of active blade pitch-control using the real-time inflow velocities including tower motions, as compared with a passive control strategy in which the blade pitch is set using only the mean wind speed.

9 Acknowledgements

This work was supported by the National Science Foundation, Division of Civil and Mechanical Systems under Agreement Number CMS-0448730 and by the Division of Power, Controls and Adaptive Networks, agreement number PCAN-1133682. Any opinions, findings, and conclusions or recommendations expressed in this material are those of the authors and do not necessarily reflect the view of the National Science Foundation.

References

- [1] J. Jonkman, "Definition of the floating system for phase IV of OC3," Tech. Rep. NREL/TP-500-47535, NREL National Energy Renewal Laboratory, 2010.
- [2] A. R. Henderson and J. H. Vugts, "Prospects for floating offshore wind energy," in *Proceedings of the European Wind Energy Conference*, 2001.
- [3] J. M. Jonkman and M. L. J. Buhl, "Fast user's guide," Tech. Rep. NREL/EL-500-38230, National Renewable Energy Laboratory, 2005.
- [4] J. M. Jonkman, "Dynamic modeling and loads analysis of an offshore floating wind turbine," Tech. Rep. NREL/TP-500-41958, NREL National Energy Renewal Laboratory, 2007.
- [5] WAMIT 4.0, *WAMIT: A Radiation-Diffraction Panel Program for Wave-Body Interactions—User's Manual*. Dept. of Ocean Engineering, M.I.T., 1995.
- [6] E. Stoneking, "Newton-euler dynamic equations of motion for a multi-body spacecraft," pp. 1368–1380, AIAA Guidance, Navigation, and Control Conference, 2007.
- [7] S. Saha, "Dynamics of serial multibody systems using the decoupled natural orthogonal complement matrices," *Journal of Applied Mechanics*, vol. 66, no. 4, pp. 986–996, 1999.
- [8] H. Matsukuma and T. Utsunomiya, "Motion analysis of a floating offshore wind turbine considering rotor-rotation," *The IES Journal Part A: Civil and Structural Engineering*, vol. 1, no. 4, pp. 268–279, 2008.
- [9] M. A. Abkowitz, *Stability and Motion Control of Ocean Vehicles*. M.I.T. Press, 1969.
- [10] R. C. Hibbeler, *Engineering Mechanics - Statics and Dynamics*. Pearson Prentice Hall, 2004.
- [11] X. H. Zeng and X. P. Shen, "Nonlinear dynamics response of floating circular cylinder with taut tether," pp. 218–224, the Proceedings of Fifteenth Offshore and Polar Engineering Conference, 2005.
- [12] A. R. Henderson and P. W. Cheng, "Wave loads and slender offshore structures, comparison of theory & measurement," in *Proceedings of the 6th German wind energy conference "Where industry meets science"*, 2002.
- [13] B. Sweetman and L. Wang, "Large-angle rigid body dynamics of a floating offshore wind turbine using euler's equations of motion," NSF CMMI Research and Innovation Conference: Engineering for Sustainability and Prosperity, 2011.
- [14] F. G. Nielsen, T. D. Hanson, and B. Skaare, "Integrated dynamic analysis of floating offshore wind turbines," in *Proceedings of the international Conference on Offshore Mechanics and Arctic Engineering*, 2006.
- [15] T. Sarpkaya and M. Issacson, *Mechanics of Wave Forces on Offshore Structures*. Van Nostrand Reinhold Company, 1981.
- [16] N. Kelley and B. Jonkman, "NWTC design codes (Turbsim)," Tech. Rep. <http://wind.nrel.gov/designcodes/>, National Renewable Energy Lab, 2008.